IEEE Access
Multidisciplinary | Rapid Review | Open Access Journal

Received August 2, 2017, accepted August 25, 2017, date of publication August 30, 2017, date of current version September 27, 2017.

Digital Object Identifier 10.1109/ACCESS.2017.2747129

Rate Region Analysis in a Full-Duplex-Aided Cooperative Nonorthogonal Multiple-Access System

HONGJI HUANG, JIAN XIONG, JIE YANG, GUAN GUI, (Member, IEEE), AND HIKMET SARI, (Fellow, IEEE)

College of Telecommunication and Information Engineering, Nanjing University of Posts and Telecommunications, Nanjing 21003, China

Corresponding author: Guan Gui (guiguan@njupt.edu.cn)

This work was supported in part by the National Natural Science Foundation of China under Grant 61401069, in part by the Jiangsu Specially Appointed Professor under Grant RK002STP16001, in part by the Jiangsu high-level creative Talent under Grant CZ0010617002, in part by the High-level Talent startup grant of the Nanjing University of Posts and Telecommunications under Grant XK0010915026, and in part by "1311 Talent Plan" of the Nanjing University of Posts and Telecommunications.

ABSTRACT Nonorthogonal multiple access (NOMA) with successive interference cancellation is considered as one of the most promising schemes in multi-user access wireless networks. Based on the principles of NOMA and full-duplex (FD) communications, this paper proposes a novel FD-aided cooperative NOMA (FD-NOMA) scheme to optimize the maximum achievable rate region. Since self-interference often exists in FD communications, a self-interference canceller is employed in this system. Specifically, three schemes that aim to maximize the achievable rate region are provided. The first one is investigated under the assumption that the transmitted power is fixed, while the other two schemes are achieved with the aid of two developed algorithms. For the purpose of studying the rate region in the non-ideality condition, the error vector magnitudelevel is introduced in the analysis of the third scheme. Finally, analytical results demonstrate that the proposed FD-NOMA scheme outperforms the conventional schemes based on NOMA in terms of the rate region, and the maximum rate region of the FD-NOMA scheme is compared with different coefficients.

INDEX TERMS Nonorthogonal multiple access (NOMA), full-duplex (FD) communications, rate region.

I. INTRODUCTION

The anticipated 1000-fold explosive data traffic growth by 2020 will lead to great challenges in the design of fifth generation communication systems (5G), and the data rate enhancement aspect has been regarded as a key issue in 5G [1]. This vital principle has promoted a large amount of research among academic and industry communities [2]–[5]. Some fundamental work investigated communications, caching, and computing oriented small cell networks, which are regarded as an important trend of 5G [6]. Nonorthogonal multiple access (NOMA) is considered one of the most promising techniques to improve spectral efficiency in 5G wireless communications [7]. Because it can support multiple users sharing the same time/frequency resource, it brings a higher spectral efficiency [8]. In NOMA, power domain multiplexing assisted with appropriate advanced non-linear detectors, e.g., users with better channel conditions, can be employed with successive interference cancelation (SIC) to remove the messages intended for other users before decoding their own, and NOMA can realize the capacity region of the downlink and uplink additive white Gaussian noise (AWGN) channel and significantly outperforms the orthogonal multiple access (OMA) schemes [9], [10].

In [11], the authors investigated the performance of a downlink NOMA scheme with randomly deployed users. The backscatter assisted wireless powered communication networks with NOMA were proposed in [12] and analyzed in terms of the sum-throughput, where a sum-throughput maximization problem was formulated and solved with the aid of the optimal transmission policy. Additionally, a weighted proportional fairness-based multiuser scheduling scheme has been proposed to balance the total throughput and cell-edge user throughput in [13]. For the purpose of optimizing the

sum rate aspect, a joint design of beam forming and power allocation in a downlink (DL) multiple-input multiple-output multiuser system which employs NOMA was developed [14]. To further improve the performance of NOMA, recently, new cooperative NOMA scheme designs have attracted some attention. In [15], the authors proposed a network model for studying cooperative simultaneous wireless information and power transfer (SWIPT) NOMA, and this is dedicated to achieving low outage probability and delivering superior throughput in comparison to the random selection scheme. In addition, a novel cooperative NOMA scheme was analyzed, and an approach based on user pairing was derived to reduce system complexity [16].

Recently, full-duplex (FD) wireless communication has attracted significant research interest due to its potential to double the spectral efficiency by allowing simultaneous DL and (uplink) UL transmission in the same frequency band [17]–[19]. The rate-region and the achievable sum rate of bidirectional communication links in a two-user FD system were investigated in [20] and [21], respectively. Furthermore, the author in [22] presented a resource allocation algorithm design for multicarrier nonorthogonal multiple access (MC-NOMA) systems employing an FD base station (BS) for serving multiple half-duplex DL and UL users simultaneously.

One important advantage of the NOMA concept is that a user with better channel conditions is compressed into a channel that is occupied by a user with worse channel conditions [23]. Additionally, the spectral efficiency can be further enhanced if the NOMA and the FD systems are integrated appropriately. In particular, for cooperative FD-NOMA systems, a new form of system that can realize better performance can be exploited by employing SIC at the users and at the signal transmitter. However, the design of optimal power allocation policies to achieve a better rate region performance aspect for this FD-NOMA system is more challenging than for traditional NOMA systems. Particularly, this design is more challenging when considering different channel conditions. Additionally, since NOMA transmission is enabled by SIC at the receivers, the SIC constraints, the changing transmitted power and the power allocation complicate the power allocation algorithm design. These unique challenges do not exist for the resource allocation algorithm design in traditional NOMA models. Meanwhile, for a NOMA system that deploys SIC at the signal transmitter and the users, multicarrier (MC) methods are efficient to reduce the large-scale fading. This implies that it is of great significance to employ MC in the FD-NOMA systems. Specifically, more complex noise except AWGN cannot be neglected in the FD-NOMA system aided by the MC. To the best of our knowledge, FD-NOMA systems have not yet been investigated in previous research. Therefore, the improvement in spectral efficiency and data rate introduced by cooperative FD-NOMA systems compared to conventional NOMA systems is not known, and the rate region optimization design for FD-NOMA systems has not yet been presented. Furthermore, MC has not been considered in the FD-NOMA systems, and the rate region optimization based on this idea is still not clear to us.

Motivated by the aforementioned considerations, a comprehensive study is conducted to optimize the rate region based on the NOMA scheme. The main contributions of this paper are summarized as follows.

1) To the best of our knowledge, we first consider a model that consists of both one FD NOMA user and one FD BS. Taking the advantages of the NOMA and the FD, an FD-NOMA scheme, which consists of one NOMA-strong user, one NOMA-weak user and one base station, is developed. Based on this model, SIC is considered at the base station and the NOMA- strong user.
2) Three cooperative schemes are proposed to maximize the achievable rate region in different cases. Specifically, the schemes under the assumptions of fixed transmitted power, unset transmitted power and signal corrupted by the EVM are taken into account and optimized in terms of the achievable maximum rate region aspect.

The remainder of this paper is organized as follows. In Section II, we propose an FD-aided cooperative NOMA scheme, in which the NOMA-weak user is cooperated by the NOMA-strong user with the capability of FD communications. Then, in Section III, several schemes that investigate the rate region based on the FD-NOMA scheme are presented. Numerical results for evaluating the performance of the proposed schemes are provided in Section IV, which is followed by conclusions in Section V.

II. SYSTEM MODEL

We consider a network with a single source (i.e., BS) and two users (U1 and U2), which is shown in Fig. 1. To be specific, U2 is a NOMA-strong user with the capability of full-duplex communications, and one NOMA-weak user is U1. Additionally, the BS is capable of full-duplex communications. The residual self-interference exists in the BS and U2. Due to the NOMA-strong user U2 and the BS working in the full-duplex mode, the direct transmission phase and cooperative phase can be performed simultaneously. In the direct transmission phase, U2 first decodes and cancels U1's signal by SIC before decoding its own data. In the cooperative phase, U2 transmits the decoded uplink data that intends for the BS to U1, and then, U1 combines and decodes the signals from the BS and U2. Since the NOMA-strong user U2 and the BS work in the full-duplex mode, they suffer from residual self-interference, which is caused by co-channel transmission and imperfect interference cancellation. Thus, successive interference cancellers are deployed at U1 and U2.

Assuming that a superposed signal transmitted by the BS is P and that its signal vector is denoted as s, the received signal at the BS in the k-th time slot can be

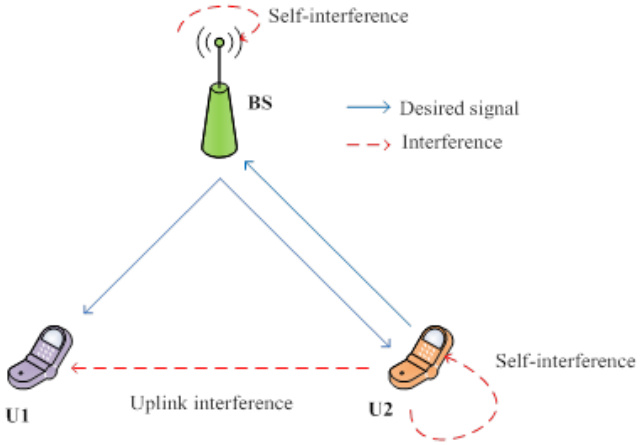

FIGURE 1. A typical example of a FD-NOMA network.

obtained as

$$y_{BS}[k]=\sqrt{P}h_{BS-BS}[k]s[k]+\sqrt{P_{2-BS}}h_{2-BS}[k]x_{2-BS}[k]+n_0 \tag{1}$$

where h_{BS-BS}, h_{2-BS}, are defined as channel coefficients of BS $\rightarrow$ BS and U2 $\rightarrow$ BS, respectively. Additionally, P_{2-BS} is the signal transmitted from U2 to the BS, and its signal vector is assumed to be x_{2-BS}. All signals are assumed to be corrupted by AWGN with zero mean and variance σ_0^2.

The NOMA-weak user, U1, receives both a downlink signal from the BS and a signal transmitted by U2; thus, the received signal is represented as

$$y_1[k] = h_1[k]\sum_{i=1}^{2}\sqrt{P_i}x_i[k]+\sqrt{P_{2-BS}}h_{2-1}[k]x_{2-BS}[k]+n_0 \tag{2}$$

In (2), h_1 and h_{2-1} are denoted as channel coefficients of BS $\rightarrow$ U1 and U2 $\rightarrow$ U1, respectively. The corresponding signal vector of h_1 is x_1. Furthermore, P_2 represents the transmitted power from BS to U2, and its signal vector is x_2. Additionally, P_1 and P_2 are denoted as the transmitted power from BS to U1 and BS to U2, respectively. Meanwhile, the NOMA-strong user, U2, receives a downlink signal from the BS and residual self-interference due to co-channel transmission, and the received signal is given by

$$y_2[k] = h_2[k]\sum_{i=1}^{2}\sqrt{P_i}x_i[k]+\sqrt{P_{2-BS}}h_{2-2}[k]x_{2-BS}[k]+n_0 \tag{3}$$

Here, h_2 and h_{2-2} represent channel coefficients of BS $\rightarrow$ U2 and U2 $\rightarrow$ U2, respectively. The received signal to interference plus noise ratio (SINR) at BS to detect x_{2-BS} is given by

$$\gamma_{BS} = \frac{P_{2-BS}\left\|h_{2-BS}\right\|^2}{P\left\|h_{BS-BS}\right\|^2+\sigma_0^2} \tag{4}$$

A. ACHIEVABLE DATA RATE AT U1

At first, considering that the channel conditions of the DL and the UL are very complex, we consider the achievable data rate at the U1 in different cases.

Theorem 1: By introducing factor ρ, the portion of decoding the DL interference dedicated by the BS $\rightarrow$ U2 can be illustrated properly.

Proof: Under the assumption, ρ indicates the portion of signal power that cannot be decoded. To be specific, $\rho = 0$ implies that x_2 can be decoded and removed successfully, while the worst case is $\rho = 1$. Afterwards, assuming the target rate of BS is R_{tol}, $(1/2)\log_2(1+\gamma_1) > R_{tol}$ is the condition that must be met for realizing decoding successfully, and we obtain

$$\gamma_1 > 2^{2R_{tol}} - 1 \tag{5}$$

Equation (5) can be rewritten as

$$\rho P_2\left\|h_1\right\|^2+\sigma_0^2 < \frac{P_1\left\|h_1\right\|^2}{2^{2R_{tol}}-1} \tag{6}$$

Thus, ρ can be formulated as

$$\rho < \frac{P_1\left\|h_1\right\|^2-(2^{2R_{tol}}-1)\sigma_0^2}{P_2\left\|h_1\right\|^2(2^{2R_{tol}}-1)} \tag{7}$$

Specifically, when x_2 can be decoded and removed totally, the corresponding relationship can be given as

$$2^{2R_{tol}} - 1 < \frac{P_1\left\|h_1\right\|^2}{\sigma_0^2} \tag{8}$$

Therefore, we can obtain the DL decoding scheme shown in Theorem 1.

Theorem 2: With the aid of the channel capacity of the link via U2 to U1, it is convenient and intuitive to illustrate the decoding strategy of the UL interference.

Proof: It is clear that the UL interference is caused by the U2$\rightarrow$BS link. To simplify this problem reasonably, we don't consider the DL interference first. Assuming that the data rate at the BS and the U1 are R_{BS} and R_1, $C_{21\max}$ and $C_{21\min}$ are noted as the channel capacities under varied conditions. Similarly, $C_{21\max}$ and $C_{21\min}$are defined as the channel capacities at BS $\rightarrow$ U1. Specifically, it can be given by

$$C_{21\max} = \frac{1}{2}\log_2\left(1+\frac{P_1\left\|h_1\right\|^2}{\sigma_0^2}\right) \tag{9}$$

$$C_{21\min} = \frac{1}{2}\log_2\left(1+\frac{P_1\left\|h_1\right\|^2}{P_{2-BS}\left\|h_{2-1}\right\|^2+\sigma_0^2}\right) \tag{10}$$

Here, when R_{BS} exceeds $C_{21\max}$, U1 cannot correctly decode the entire signal from U2 even though there is no interference from BS under our assumption. Hence, the signal from U2 is just treated as noise by U1 in this case. By contrast, when $R_{BS} \leq C_{21\min}$, SIC can be employed at the U1, which can totally mitigate the UL interference. Furthermore, if $C_{21\min} \leq R_{BS} \leq C_{21\max}$, the UL interference can be partly removed. Thus, the proof of Theorem 2 is completed.

Based on our analysis, the achievable data rate at the U1 is given as

$$R_1 = \begin{cases} \frac{1}{2}\log_2\left(1+\frac{P_1\|h_1\|^2}{\sigma_0^2}\right), \\ R_{BS} \le C_{12\min}, \quad R_2 \le C_{1\min} \\ \frac{1}{2}\log_2\left(1+\frac{P_1\|h_1\|^2}{P_2\|h_1\|^2+\sigma_0^2}\right), \\ R_{BS} \le C_{12\min}, \quad R_2 \ge C_{1\max} \\ \frac{1}{2}\log_2\left(1+\frac{P_1\|h_1\|^2}{\rho P_2\|h_1\|^2+\sigma_0^2}\right), \\ R_{BS} \le C_{12\min}, \quad C_{1\min} \le R_2 \le C_{1\max} \\ \frac{1}{2}\log_2\left(1+\frac{P_1\|h_1\|^2}{P_{2-BS}\|h_{2-1}\|^2+\rho P_2\|h_1\|^2+\sigma_0^2}\right), \\ R_{BS} \ge C_{12\max}, \quad C_{1\min} \le R_2 \le C_{1\max} \\ \frac{1}{2}\log_2\left(1+\frac{P_1\|h_1\|^2}{P_{2-BS}\|h_{2-1}\|^2+P_2\|h_1\|^2+\sigma_0^2}\right), \\ R_{BS} \ge C_{12\max}, \quad R_2 \ge C_{1\max} \\ \frac{1}{2}\log_2\left(1+\frac{P_1\|h_1\|^2+P_{2-BS}\|h_{2-1}\|^2}{P_2\|h_1\|^2+\sigma_0^2}\right)-R_{BS}, \\ C_{12\min} \le R_{BS} \le C_{12\max}, \quad R_2 \ge C_{1\max} \\ \frac{1}{2}\log_2\left(1+\frac{P_1\|h_1\|^2+P_{2-BS}\|h_{2-1}\|^2}{\sigma_0^2}\right)-R_{BS}, \\ C_{12\min} \le R_{BS} \le C_{12\max}, \quad R_2 \le C_{1\min} \\ \frac{1}{2}\log_2\left(1+\frac{P_1\|h_1\|^2+P_{2-BS}\|h_{2-1}\|^2}{\rho P_2\|h_1\|^2+\sigma_0^2}\right)-R_{BS}, \\ C_{12\min} \le R_{BS} \le C_{12\max}, \quad C_{1\min} \le R_2 \le C_{1\max} \end{cases} \tag{11}$$

B. ACHIEVABLE DATA RATE AT U2

In this subsection, we present the achievable data rate at the U2. With the aid of Theorem 1 and Theorem 2, the data rate of the U2 can be given as

$$R_2 = \begin{cases} \frac{1}{2}\log_2\left(1+\frac{P_2\|h_2\|^2}{P_{2-BS}\|h_{2-2}\|^2+\sigma_0^2}\right), \\ R_2 \ge C_{1\max} \\ \frac{1}{2}\log_2\left(1+\frac{P_2\|h_2\|^2}{P_{2-BS}\|h_{2-2}\|^2+P_1\|h_2\|^2+\sigma_0^2}\right), \\ R_2 \le C_{1\min} \\ \frac{1}{2}\log_2\left(1+\frac{P_2\|h_2\|^2}{P_{2-BS}\|h_{2-2}\|^2+(1-\rho)P_1\|h_2\|^2+\sigma_0^2}\right), \\ C_{1\min} \le R_2 \le C_{1\max} \end{cases} \tag{12}$$

Additionally, the achievable data rates of BS can be given as follows

$$R_{BS} = \frac{1}{2}\log_2(1+\gamma_{BS}) = \frac{1}{2}\log_2\left(1+\frac{P_{2-BS}\|h_{2-BS}\|^2}{P\|h_{BS-BS}\|^2+\sigma_0^2}\right) \tag{13}$$

III. ACHIEVABLE RATE REGION ANALYSIS BASED ON FD-NOMA SCHEMES

In this section, based on the proposed FD-NOMA network and principles of the rate region, the achievable rates of the base station and users are given for FD-NOMA systems. To be specific, for the purpose of maximizing the rate region, three schemes based on NOMA are presented. Furthermore, optimal power allocation solutions are provided.

A. RATE REGION WHEN THE TRANSMITTED POWER IS FIXED

The SIC detection is deployed at the BS and the U2 in the synchronous NOMA scheme. In particular, BS first decodes x_{2-BS} and subtracts the self-interference. Then, U2 can directly decode x_2 while considering x_{2-BS}as noise. Assuming successful decoding and no error propagation, the achievable rate region of BS and two users can be given in different cases based on the channel conditions.

Case 1: $R_{BS} \le C_{12\min}, R_2 \le C_{1\min}$.

$$\begin{cases} 0 \le R_{BS} \le \frac{1}{2}\log_2\left(1+\frac{P_{2-BS}\|h_{2-BS}\|^2}{P\|h_{BS-BS}\|^2+\sigma_0^2}\right) \\ 0 \le R_1 \le \frac{1}{2}\log_2\left(1+\frac{P_1\|h_1\|^2}{\sigma_0^2}\right) \\ 0 \le R_2 \le \frac{1}{2}\log_2 \\ \quad \times\left(1+\frac{P_2\|h_2\|^2}{P_{2-BS}\|h_{2-2}\|^2+P_1\|h_2\|^2+\sigma_0^2}\right) \end{cases} \tag{14}$$

Case 2: $R_{BS} \le C_{12\min}, R_2 \ge C_{1\max}$.

$$\begin{cases} 0 \le R_{BS} \le \frac{1}{2}\log_2\left(1+\frac{P_{2-BS}\|h_{2-BS}\|^2}{P\|h_{BS-BS}\|^2+\sigma_0^2}\right) \\ 0 \le R_1 \le \frac{1}{2}\log_2\left(1+\frac{P_1\|h_1\|^2}{P_2\|h_1\|^2+\sigma_0^2}\right) \\ 0 \le R_2 \le \frac{1}{2}\log_2\left(1+\frac{P_2\|h_2\|^2}{P_{2-BS}\|h_{2-2}\|^2+\sigma_0^2}\right) \end{cases} \tag{15}$$

Case 3: $R_{BS} \le C_{12\min}, C_{1\min} \le R_2 \le C_{1\max}$.

$$\begin{cases} 0 \le R_{BS} \le \frac{1}{2}\log_2\left(1+\frac{P_{2-BS}\|h_{2-BS}\|^2}{P\|h_{BS-BS}\|^2+\sigma_0^2}\right) \\ 0 \le R_1 \le \frac{1}{2}\log_2\left(1+\frac{P_1\|h_1\|^2}{\rho P_2\|h_1\|^2+\sigma_0^2}\right) \\ 0 \le R_2 \le \frac{1}{2}\log_2 \\ \quad \times\left(1+\frac{P_2\|h_2\|^2}{P_{2-BS}\|h_{2-2}\|^2+(1-\rho)P_1\|h_2\|^2+\sigma_0^2}\right) \end{cases} \tag{16}$$

Case 4: $R_{BS} \geq C_{12\min}$, $C_{1\min} \leq R_2 \leq C_{1\max}$.

$$\begin{cases} 0 \leq R_{BS} \leq \frac{1}{2}\log_2\left(1+\frac{P_{2-BS}\left\|h_{2-BS}\right\|^2}{P\left\|h_{BS-BS}\right\|^2+\sigma_0^2}\right) \\ 0 \leq R_1 \leq \frac{1}{2}\log_2\left(1+\frac{P_1\left\|h_1\right\|^2}{P_{2-BS}\left\|h_{2-1}\right\|^2+\rho P_2\left\|h_1\right\|^2+\sigma_0^2}\right) \\ 0 \leq R_2 \leq \frac{1}{2}\log_2 \\ \quad \times\left(1+\frac{P_2\left\|h_2\right\|^2}{P_{2-BS}\left\|h_{2-2}\right\|^2+(1-\rho)P_1\left\|h_2\right\|^2+\sigma_0^2}\right) \end{cases} \tag{17}$$

Case 5: $R_{BS} \geq C_{12\max}$, $R_2 \geq C_{1\max}$.

$$\begin{cases} 0 \leq R_{BS} \leq \frac{1}{2}\log_2\left(1+\frac{P_{2-BS}\left\|h_{2-BS}\right\|^2}{P\left\|h_{BS-BS}\right\|^2+\sigma_0^2}\right) \\ 0 \leq R_1 \leq \frac{1}{2}\log_2\left(1+\frac{P_1\left\|h_1\right\|^2}{P_{2-BS}\left\|h_{2-1}\right\|^2+P_2\left\|h_1\right\|^2+\sigma_0^2}\right) \\ 0 \leq R_2 \leq \frac{1}{2}\log_2\left(1+\frac{P_2\left\|h_2\right\|^2}{P_{2-BS}\left\|h_{2-2}\right\|^2+\sigma_0^2}\right) \end{cases} \tag{18}$$

Case 6: $C_{12\min} \leq R_{BS} \leq C_{12\max}$, $R_2 \geq C_{1\max}$.

$$\begin{cases} 0 \leq R_{BS} \leq \frac{1}{2}\log_2\left(1+\frac{P_{2-BS}\left\|h_{2-BS}\right\|^2}{P\left\|h_{BS-BS}\right\|^2+\sigma_0^2}\right) \\ 0 \leq R_1 \leq \frac{1}{2}\log_2\left(1+\frac{P_1\left\|h_1\right\|^2+P_{2-BS}\left\|h_{2-1}\right\|^2}{P_2\left\|h_1\right\|^2+\sigma_0^2}\right)-R_{BS} \\ 0 \leq R_2 \leq \frac{1}{2}\log_2\left(1+\frac{P_2\left\|h_2\right\|^2}{P_{2-BS}\left\|h_{2-2}\right\|^2+\sigma_0^2}\right) \end{cases} \tag{19}$$

Case 7: $C_{12\min} \leq R_{BS} \leq C_{12\max}$, $R_2 \leq C_{1\min}$.

$$\begin{cases} 0 \leq R_{BS} \leq \frac{1}{2}\log_2\left(1+\frac{P_{2-BS}\left\|h_{2-BS}\right\|^2}{P\left\|h_{BS-BS}\right\|^2+\sigma_0^2}\right) \\ 0 \leq R_1 \leq \frac{1}{2}\log_2\left(1+\frac{P_1\left\|h_1\right\|^2+P_{2-BS}\left\|h_{2-1}\right\|^2}{P_2\left\|h_1\right\|^2+\sigma_0^2}\right)-R_{BS} \\ 0 \leq R_2 \leq \frac{1}{2}\log_2\left(1+\frac{P_2\left\|h_2\right\|^2}{P_{2-BS}\left\|h_{2-2}\right\|^2+P_1\left\|h_2\right\|^2+\sigma_0^2}\right) \end{cases} \tag{20}$$

Case 8: $C_{12\min} \leq R_{BS} \leq C_{12\max}$, $C_{1\min} \leq R_2 \leq C_{1\max}$.

$$\begin{cases} 0 \leq R_{BS} \leq \frac{1}{2}\log_2\left(1+\frac{P_{2-BS}\left\|h_{2-BS}\right\|^2}{P\left\|h_{BS-BS}\right\|^2+\sigma_0^2}\right) \\ 0 \leq R_1 \leq \frac{1}{2}\log_2\left(1+\frac{P_1\left\|h_1\right\|^2+P_{2-BS}\left\|h_{2-1}\right\|^2}{P_2\left\|h_1\right\|^2+\sigma_0^2}\right)-R_{BS} \\ 0 \leq R_2 \leq \frac{1}{2}\log_2 \\ \quad \times\left(1+\frac{P_2\left\|h_2\right\|^2}{P_{2-BS}\left\|h_{2-2}\right\|^2+(1-\rho)P_1\left\|h_2\right\|^2+\sigma_0^2}\right) \end{cases} \tag{21}$$

To maximize the achievable rate region related to (14)-(21), an optimization problem is formulated as

$$\begin{aligned} \underset{P_1,P_2}{\text{maxmize}}\ & \vec{\mu}\cdot\vec{R} = \mu_1 R_{BS}+\mu_2 R_1+\mu_3 R_2 \\ \text{subject to C1: } & \sum_{i=1}^{2} P = P_0 \\ \text{C2: } & \sum_{i=1}^{3}\mu_i = 1 \\ \text{C3: } & P\gamma_{BS} \geq P_{2-BS}\gamma_2 \\ \text{C4: } & P_1\gamma_2 \geq P_1\gamma_1 \\ \text{C5: } & P_i \geq 0, \quad \forall i = 1,2 \end{aligned} \tag{22}$$

where μ_i $(\forall i)$ can be denoted as the weight coefficient of the data rates of BS, U1 and U2, and we can change the achievable rate region by adopting μ_i. Additionally, C3 and C4 are the SIC constraints of BS and U2, in which γ_1 and γ_2 are assumed to be the SINR of U1 and U2. Additionally, P_0 is denoted as the maximum transmitted power threshold. Then, we introduce the power allocation factor α, and (22) can be rewritten as

$$\begin{aligned} \underset{\alpha}{\text{maxmize}}\ & \vec{\mu}\cdot\vec{R} = \mu_1 R_{BS}+\mu_2 R_1+\mu_3 R_2 \\ \text{subject to C1: } & \sum_{i=1}^{2} P_i = P_0, \alpha \in [0,1] \\ \text{C2: } & \sum_{i=1}^{3}\mu_i = 1 \\ \text{C3: } & P\gamma_{BS} \geq P_{2-BS}\gamma_2 \\ \text{C4: } & P_1\gamma_2 \geq P_1\gamma_1 \\ \text{C5: } & P_0 \geq 0 \end{aligned} \tag{23}$$

In (14)-(21), we observe that it is a convex problem (the proof is given in the Appendix) for any fixed factors P_0 and thus can be solved by introducing *Lagrangian duality optimization*. Hence, we construct the sub problem of Lagrangian relaxation in (15).

$$\begin{aligned} \underset{\alpha,\lambda}{\text{maxmize}}\ & L(\alpha,\lambda) = \mu_1 R_{BS}+\mu_2 R_1+\mu_3 R_2 \\ & \quad +\lambda(\alpha P_0\gamma_2-\alpha P_0\gamma_1) \\ \text{subject to: C1, C2, C3, C5} & \end{aligned} \tag{24}$$

With the aid of off-the-shelf solvers, e.g., CVX [24], the optimal solution can be obtained. Additionally, in order to ensure the performance of NOMA systems, the NOMA-strong user U2 is allocated less power than the NOMA-weak user U1. Thus, taking case 1 as an example, the solution can be obtained as

$$\begin{aligned} \alpha &= \frac{\sqrt{(b+ac)^2+4ab^2}-b-ac}{2ab} \\ &= (b+ac)\times\frac{\sqrt{1+\frac{4ab^2}{(b+ac)^2}}-1}{2ab} \end{aligned} \tag{25}$$

where $a = \|h_1\|/\sigma_0^2, b = \|h_2\|^2$ and $c = P_{2-BS}\|h_{2-2}\|^2 + \sigma_0^2$. Specially, when the channel condition of the BS $\rightarrow$ U2 link is very poor, power allocation factor α is approximated as

$$\alpha = \lim_{\frac{4ab^2}{(b+ac)^2}\rightarrow 0} (b+ac) \times \frac{\sqrt{1+\frac{4ab^2}{(b+ac)^2}}-1}{2ab} \approx \frac{b}{b+ac} \tag{26}$$

By contrast, considering another case that $\|h_2\|^2 \gg \|h_1\|^2$, we obtain

$$\begin{aligned}\alpha &= (b+ac) \times \frac{\sqrt{1+\lim_{b\rightarrow\propto}\frac{4ab^2}{(b+ac)^2}}-1}{2ab} \\ &\approx \lim_{b\rightarrow\propto}(b+ac) \times \frac{\sqrt{1+4a}-1}{2ab} \\ &\approx \frac{\sqrt{1+4a}-1}{2a}\end{aligned} \tag{27}$$

Additionally, it is worth noting that c can be adopted as $c = \rho P_{2-BS}\|h_{2-2}\|^2 + \sigma_0^2$in other channel conditions. Therefore, the optimized power allocation scheme is formulated by employing (25) in the transmitted power initiation. Similarly, since case 2 to case 8 are convex problems, it is easy to formulate an optimal solution through the same method as Case 1.

B. RATE REGION WHEN THE TRANSMITTED POWER IS NOT FIXED

This subsection presents the achievable rate region for an FD-NOMA scheme with changing transmitted power P_0. To be specific, this scheme considers eight different channel conditions as illustrated in (14)-(21). Accordingly, we formulate a rate region maximization problem as

$$\begin{aligned}&\underset{P_1,P_2,P,P_{2-BS}}{\text{maxmize}} \ \vec{\mu}\cdot\vec{R} = \mu_1 R_{BS} + \mu_2 R_1 + \mu_3 R_2 \\ &\text{subject to C1: } \sum_{i=1}^{2} P_i \le P_0 \\ &\qquad \text{C2: } \sum_{i=1}^{3}\mu_i = 1 \\ &\qquad \text{C3: } P\gamma_{BS} \ge P_{2-BS}\gamma_2 \\ &\qquad \text{C4: } P_1\gamma_2 \ge P_1\gamma_1 \\ &\qquad \text{C5: } P_i, P_{2-BS} \ge 0, \quad \forall i = 1,2\end{aligned} \tag{28}$$

Similar to the maximization problem in (23), (28) can be further expressed as

$$\begin{aligned}&\underset{\alpha,P,P_{2-BS}}{\text{maxmize}} \ \vec{\mu}\cdot\vec{R} = \mu_1 R_{BS} + \mu_2 R_1 + \mu_3 R_2 \\ &\text{subject to C1: } \sum_{i=1}^{2} P_i \le P_0, \quad \alpha \in [0,1] \\ &\qquad \text{C2: } \sum_{i=1}^{3}\mu_i = 1 \\ &\qquad \text{C3: } P\gamma_{BS} \ge P_{2-BS}\gamma_2 \\ &\qquad \text{C4: } P_1\gamma_2 \ge P_1\gamma_1 \\ &\qquad \text{C5: } P_0, P_{2-BS} \ge 0\end{aligned} \tag{29}$$

Generally, the problem above is non-convex. Note that in complexity theory, non-convexity of a formulation proves the problem's hardness, as a problem could not be appropriately formulated. However, since (29) is formulated in the NOMA system under the assumption that the strong NOMA user U2 has a better channel condition than the weak NOMA user U1, we present an algorithm to solve this problem.

Though (29) is a non-convex problem, we can obtain the optimal solution with the aid of the concept of DC programming (difference of the convex functions). DC programming is a branch of algorithms that can be employed in optimization problems among cognitive radio, electronic technology and other fields. CCCP (Concave-convex Procedure) is a method based on the DC concept. Taking the advantages of a CCCP algorithm, we develop a scheme to solve (29), which can also be rewritten as

$$\begin{aligned}&\underset{\alpha,P,P_{2-BS}}{\text{minimize}} \ H(\alpha,P,P_{2-BS}) - Y(\alpha,P,P_{2-BS}) \\ &\text{subject to C1: } \sum_{i=1}^{2} P_i \le P_0, \quad \alpha \in [0,1] \\ &\qquad \text{C2: } \sum_{i=1}^{3}\mu_i = 1 \\ &\qquad \text{C3: } P\gamma_{BS} \ge P_{2-BS}\gamma_2 \\ &\qquad \text{C4: } P_1\gamma_2 \ge P_1\gamma_1 \\ &\qquad \text{C5: } P_0, P_{2-BS} \ge 0\end{aligned} \tag{30}$$

Here, the minimizing terms are defined as $H(\alpha, P, P_{2-BS}) = -\mu_2 R_1 - \mu_3 R_2$ and $Y(\alpha, P, P_{2-BS}) = -\mu_1 R_{BS}$, respectively. First, for the purpose of measuring the performance of the algorithm, an error propagation function *Error* is defined, which can be formulated as

$$Error = \|opt_{n+1} - opt_n\|_2 \tag{31}$$

where n is denoted as the number of iterations. Additionally, opt_n is assumed to be the solution in n-th iteration. Then, as is illustrated in Algorithm 1, the algorithm for optimizing the maximum rate region problem is presented. Hence, with the aid of the proposed Algorithm 1, the optimal solution of the rate region is obtained when the transmitted power is not fixed.

C. RATE REGION WHEN THE TRANSMITTED POWER IS CORRUPTED BY EVM

As indicated in [25] and [26], a great challenge in FD communications is induced by non-ideal transceiver implementation. For a practical communication link, the non-ideality such as phase noise of local oscillators, non-linearity of amplifiers and so on leads to severe deviation from their ideal locations.

Algorithm 1 Calculating Maximum Rate Region Based on CCCP Method

(1) **Initialization**: Set $P = 0$, $P_{2-BS} = 0$, $\alpha = 0$, $l_\alpha = 0.01$, $l_{P_{2-BS}} = 0.02$, $l_P = 0.05$, $n_\alpha = 0$,, $n_{P_{2-BS}} = 0$, $n_P = 0$, $\xi = 0.005$. Here, l_α, $l_{P_{2-BS}}$, l_P are assumed as the step of α, P_{2-BS} and P during the iteration process, respectively. n_α, $n_{P_{2-BS}}$, n_P are assumed as the number of iteration of α, P_{2-BS} and P. Furthermore, ξ represents the accuracy of the algorithm.

(2) Calculating an auxiliary function $\hat{f}^{(l_\alpha, l_{P_{2-BS}}, l_P)} H(\alpha, P, P_{2-BS}) - Y(\alpha, P, P_{2-BS})^{(l_\alpha, l_{P_{2-BS}}, l_P)} + z^T_{(l_\alpha, l_{P_{2-BS}}, l_P)}$, where $z^T_{(l_\alpha, l_{P_{2-BS}}, l_P)} \in \partial h(\alpha, P, P_{2-BS})^{(l_\alpha, l_{P_{2-BS}}, l_P)}$.

(3) **If** $Error \leq \xi$ ($Error$ is calculated by (22)), the optimal solution opt_n is obtained. Specifically, opt_nconsists of the solution of α, P_{2-BS} and P, and opt_n is the maximum rate region of the proposed FD-NOMA system. After that, turn to 6).

(4) **If** $Error > \xi$, then

$$\begin{aligned}
&\alpha \leftarrow \alpha + l_\alpha,\\
&P_{2-BS} \leftarrow l_{P_{2-BS}},\\
&P \leftarrow l_P,\\
&n_\alpha \leftarrow n_\alpha + 1,\\
&n_{P_{2-BS}} \leftarrow n_{P_{2-BS}} + 1,\\
&n_P \leftarrow n_P + 1.
\end{aligned}$$

After that, turn to step (2).

(5) **If** $\alpha = 0.99$, turn to next step (6).

(6) **Output**: opt_n, α, P_{2-BS}, P and n $= \max\{n_\alpha, n_{P_{2-BS}}, n_P\}$.

(7) **End**

This deviation is quantified in general by a measure called the Error Vector Magnitude (EVM) level. Therefore, as an FD system, it is necessary for us to investigate the rate region for the transmitted power with EVM corruption. Meanwhile, the MC communication system is introduced to overcome frequency selective fading. Therefore, a FD-NOMA system corrupted by an EVM noise added to the original signal at the transmission on each sub-carrier is developed.

Thus, referring to [26], assuming that added EVM noise is η on m sub-carrier index, we obtain

$$\gamma^E_{BS} = \frac{E\left\{|s[m]|^2\right\}}{E\left\{|\eta[m]|^2\right\}} \tag{32}$$

$$\gamma^E_1 = \frac{E\left\{|x_1[m]|^2\right\}}{E\left\{|\eta[m]|^2\right\}} \tag{33}$$

$$\gamma^E_2 = \frac{E\left\{|x_2[m]|^2\right\}}{E\left\{|\eta[m]|^2\right\}} \tag{34}$$

Here, (32) is assumed as the EVM of the BS, while (33) and (34) are defined as that of U1 and U2. Thus, when the channel condition from U1 to U2 is good, the rate region can be expressed as

$$\begin{cases}
0 \leq R_{BS} \leq \frac{1}{2}\sum_{m=1}^{M} \log_2 \\
\quad \times \left(1 + \frac{x_{2-BS}[m]\gamma^E_{BS}\|h_{2-BS}[m]\|^2}{P\|h_{BS-BS}[m]\|^2 + \sigma_0^2(1+\gamma^E_{BS})}\right)\\
0 \leq R_1 \leq \frac{1}{2}\sum_{m=1}^{M} \log_2\left(1 + \frac{x_1[m]\gamma^E_1\|h_1[m]\|^2}{x_2[m]\|h_1[m]\|^2 + \sigma_0^2(1+\gamma^E_1)}\right)\\
0 \leq R_2 \leq \frac{1}{2}\sum_{m=1}^{M} \log_2 \\
\quad \times \left(1 + \frac{x_2[m]\gamma^E_2\|h_2[m]\|^2}{P_{2-BS}\|h_{2-2}[m]\|^2 + \sigma_0^2(1+\gamma^E_2)}\right)
\end{cases} \tag{35}$$

In (35), M represents the total number of the sub-carriers. Additionally, $x_{2-BS}[m]$, $x_1[m]$ and $x_2[m]$ are defined as each sub-carrier of U2 $\rightarrow$ BS, BS $\rightarrow$ U1 and BS $\rightarrow$ U2, respectively. Consider that if the channel condition becomes worse, the rate region is written as

$$\begin{cases}
0 \leq R_{BS} \leq \frac{1}{2}\sum_{m=1}^{M} \log_2 \\
\quad \times \left\{1 + \frac{\gamma^E_{BS}x_{2-BS}[m]\|h_{2-BS}[m]\|^2}{P\|h_{BS-BS}[m]\|^2 + \sigma_0^2(1+\gamma^E_{BS})}\right\}\\
0 \leq R_1 \leq \frac{1}{2}\sum_{m=1}^{M} \log_2 \\
\left\{1 + \frac{\gamma^E_1 x_1[m]\|h_1[m]\|^2}{x_2[m]\|h_1[m]\|^2 + P_{2-BS}\|h_{2-1}[m]\|^2 + \sigma_0^2(1+\gamma^E_1)}\right\}\\
0 \leq R_2 \leq \frac{1}{2}\sum_{m=1}^{M} \log_2 \\
\quad \times \left\{1 + \frac{\gamma^E_2 x_2[m]\|h_2[m]\|^2}{P_{2-BS}\|h_{2-2}[m]\|^2 + \sigma_0^2(1+\gamma^E_2)}\right\}
\end{cases} \tag{36}$$

Based on (35) and (36), the corresponding rate region maximization problem is then formulated as

$$\begin{aligned}
\underset{x_1,x_2,P,P_{2-BS}}{\text{maxmize}} \quad & \overrightarrow{\mu}\cdot\overrightarrow{R} = \mu_1 R_{BS} + \mu_2 R_1 + \mu_3 R_2\\
\text{subject to C1:} \quad & \sum_{m=1}^{M}(x_1[m] + x_2[m]) \leq P_0\\
\text{C2:} \quad & \sum_{i=1}^{3}\mu_i = 1\\
\text{C3:} \quad & P\gamma_{BS} \geq \sum_{m=1}^{M} x_{2-BS}[m]\gamma_2\\
\text{C4:} \quad & \sum_{m=1}^{M} x_1[m]\gamma_2 \geq \sum_{m=1}^{M} x_2[m]\gamma_2\\
\text{C5:} \quad & x_i[m] \geq 0, \quad \forall\\
\text{C6:} \quad & P_{2-BS} \geq 0
\end{aligned} \tag{37}$$

Algorithm 2 Calculating Maximum Rate Region via DFP Method.

(1) **Initialization**: Set $x_1[m] = 0, x_2[m] = 0, P_{2-BS} = 0, \alpha = 0, \xi = 0.005$. Here, we define $solution^{(1)} = \{x_1[m], x_2[m], P_{2-BS}0, \alpha$, and set $solution^{(1)} \in R^n$. Specifically, n is the number of iterations, while ξ represents the accuracy.

(2) Set $H_1 = I_n$, and the gradient can be obtained as $g_1 = \nabla f(solution^{(1)})$ where k is set as 1.

(3) Calculate $d^{(k)} = -H_k g_k$.

(4) Try to get the step υ_k, which can be given by $f\left(solution^{(1)} + \upsilon_k d^{(k)}\right) = minf\left(solution^{(1)} + \upsilon d^{(k)}\right)$, where $solution^{(k+1)} = solution^{(1)} + \upsilon_k d^{(k)}$.

(5) **If** $\left\|\nabla f(solution^{(k+1)})\right\| \leq \zeta$, the optimal solution $solution = solution^{(k+1)}$ is obtained.
Else $\left\|\nabla f(solution^{(k+1)})\right\| > \zeta$, turn to step (6).

(6) **If** $k = n, solution^{(1)} \leftarrow solution^{(k+1)}$, turn to step (2).
Else turn to 7).

(7) Update $g_{k+1} = \nabla f(solution^{(k+1)})$and $p_{k+1} = solution^{(k+1)} - solution^{(k)}$.

(8) Update $q_{k+1} = g_{k+1} - g_k$, and H_{k+1} can be obtained by

$$H_{k+1} = H_k + \frac{p^{(k)} p^{(k)T}}{p^{(k)T} q^{(k)}} - \frac{H_k q^{(k)} q^{(k)T} H_k}{p^{(k)T} H_k q^{(k)}}$$

Then, set $k \leftarrow k + 1$, turn to step (3).

(9) **End**

Since solving (37) is a non-convex problem, it is difficult to obtain the optimal solution. To solve it efficiently, we introduce the penalty theory, and (37) can be modified as

$$\begin{aligned}
\underset{x_1, x_2, \alpha, P_{2-BS}}{\text{maxmize}} \quad & \overrightarrow{\mu} \cdot \overrightarrow{R} = \mu_1 R_{BS} + \mu_2 R_1 + \mu_3 R_2 \\
& + \lambda\left(\sum_{m=1}^{M} x_1[m]\gamma_2 - \sum_{m=1}^{M} x_2[m]\gamma_2\right) \\
& + \varsigma\left(P\gamma_{BS} - \sum_{m=1}^{M} x_{2-BS}[m]\gamma_2\right) \\
\text{subject to C1:} \quad & \sum_{m=1}^{M} (x_1[m] + x_2[m]) \leq P_0 \\
\text{C2:} \quad & \sum_{i=1}^{3} \mu_i = 1 \\
\text{C3:} \quad & x_i[m] \geq 0, \quad \forall \\
\text{C4:} \quad & P_{2-BS} \geq 0
\end{aligned} \tag{38}$$

From (38), we observe that this problem is still non-convex. As it is a continuous and differentiable function, the optimal solution can be solved successfully by the Davidon–Fletcher–Powell (DFP) algorithm. Eventually, an algorithm based on the DFP method is developed to optimize the maximum rate region problem formulated in (38). This algorithm is illustrated as follows.

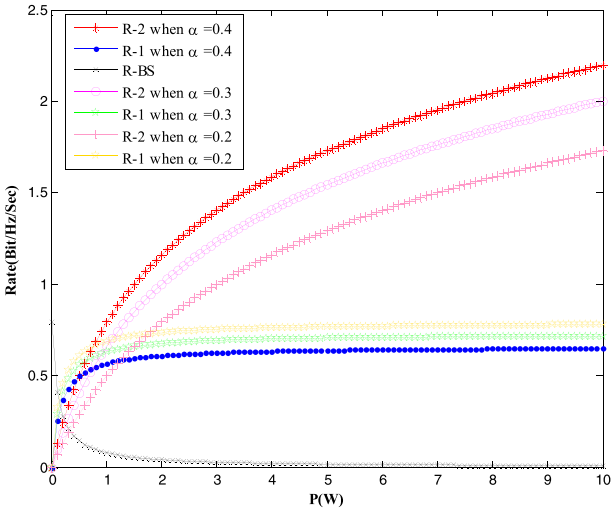

FIGURE 2. Rate region for BS, U1 and U2 with different power allocation factor α when $R_{BS} \geq C_{12max}$ and $R_2 \geq C_{1max}$.

IV. NUMERICAL RESULTS AND ANALYSIS

In this section, numerical results are presented to facilitate the performance evaluations of the proposed achievable rate region optimization problem based on the FD-NOMA system we developed. In the considered model, we assume that the transmitted power P_{2-BS} of U2 is 6 W, and its corresponding channel coefficient h_{2-BS}^2 is 4. Additionally, the channels are assumed as independently and identically distributed Rayleigh fading, of which the channel coefficients of U1 and U2 are given as $\|h_1\|^2 \leq \|h_2\|^2$, while $\|h_{2-1}\|^2 = \|h_{2-2}\|^2 = -20dB$ is considered. Moreover, we assume that the total transmit power at the BS is 0-10 dBw. Without loss of generality, we further denote that the noise level at BS, U1 and U2 are the same, i.e., $\sigma_0^2 = -10$dBm. Furthermore, ρ is changing from 0 to 1. In addition, we generate one hundred instances and consider the average performance of the proposed Algorithm 1 and Algorithm 2.

Fig. 2 shows the simulation results of the maximum achievable rate region when the transmitted power is fixed at the BS, U1 and U2. Setting P_0 as 0-10W, it can be seen from Fig. 2 that the data rate improves with the increasing transmitted power. Additionally, it can be observed that the data rate of U2 is significantly larger than that of U1. Additionally, since the constraint C3 becomes worse as the transmitted power increases, the data rate of the BS is decreases with larger transmitted power. Furthermore, Fig. 2 illustrates that R_2 of $\alpha = 0.4$ is larger than that of α is 0.2 and 0.3, while R_1 is worse in the case of bigger α. Specifically, this result is dedicated by difference power allocation of U1 and U2 with the aid of α.

Fig. 3 depicts the maximum achievable rate region when the transmitted power is not fixed for changing power allocation factor α. Here, it is noted that the maximum transmitted power is 5 W, and the rate region of the FD-NOMA system is presented based on Algorithm 1. It can be seen from Fig. 3 that the rate region is improved in the case where α is 0.4, which is dedicated by the NOMA-stronger user U2,

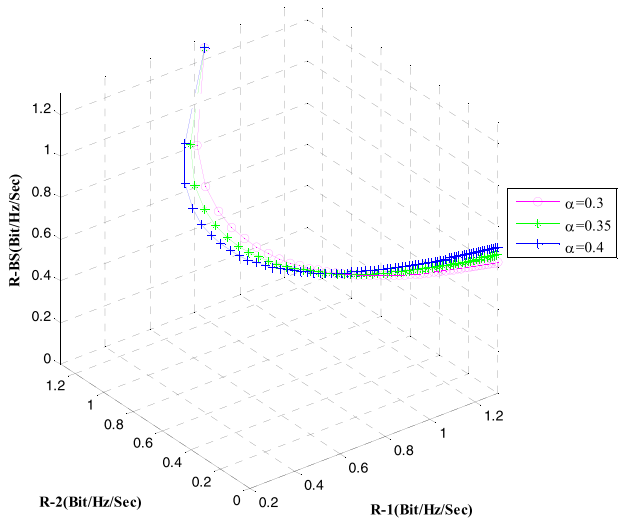

FIGURE 3. The maximum achievable rate region when the transmitted power is not fixed in the case different power allocation factor α when $R_{BS} \geq C_{12\,max}$ and $R_2 \geq C_{1\,max}$.

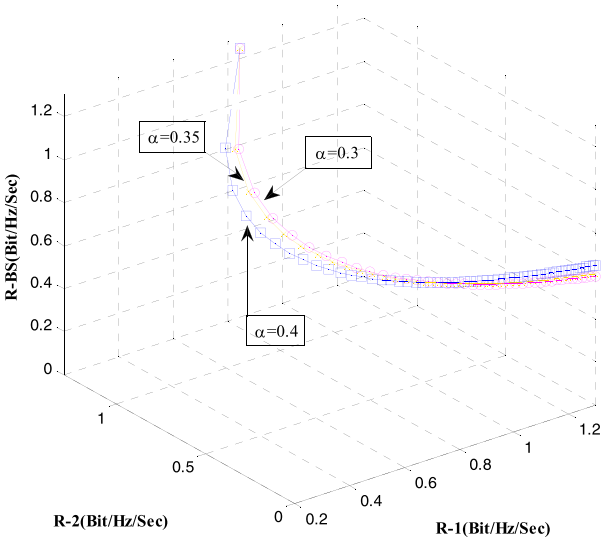

FIGURE 5. The maximum achievable rate region when the signal is corrupted by the EVM in the case of different power allocation factor α when $R_{BS} \geq C_{12\,max}$, $R_2 \geq C_{1\,max}$.

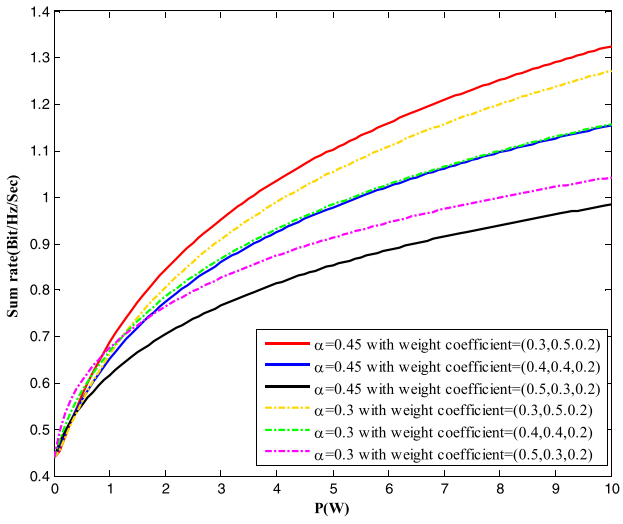

FIGURE 4. The maximum achievable rate region when the transmitted power is not fixed for different power allocation factor α and weight coefficients (μ_1, μ_2, μ_3) when $R_{BS} \geq C_{12\,max}$, $R_2 \geq C_{1\,max}$.

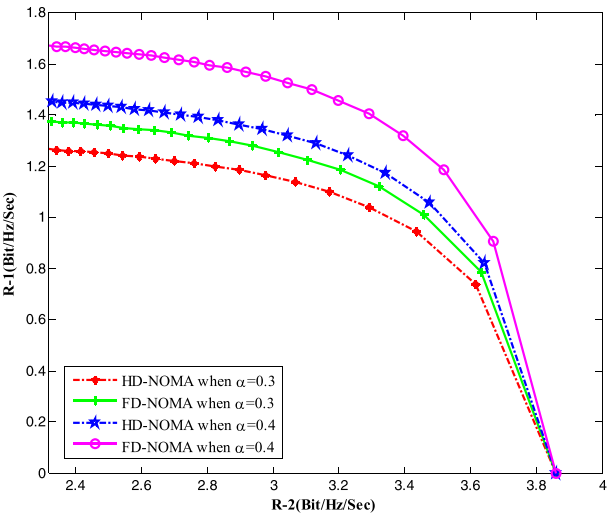

FIGURE 6. Half-duplex and full-duplex rate region comparison under different power allocation coefficient α when $R_{BS} \geq C_{12\,max}$, $R_2 \geq C_{1\,max}$.

which has more capability for decoding the signal. This result indicates that the achievable rate region can be adjusted by changing α.

In this comparison, we investigate the achievable rate region when the transmitted power is not fixed with a different weight coefficient in two cases. Noting that the signal is only corrupted by the AWGN, it can be observed from Fig. 4 that a there is a significant difference between the rate regions when setting different power coefficients at the BS, U1 and U2. For example, assuming that α is 0.45, the maximum rate region has a great improvement when the weight factor is (0.3, 0.5, 0.2) compared with that of other two cases. Additionally, it can be further seen from Fig. 4 that the weight factor has a greater impact on the rate region with a larger power allocation factor α, which indicates that adopting the power allocation factor properly can reduce the variation of the maximum rate region caused by weight factor.

Fig. 5 shows the maximum achievable rate region when the transmitted signal is corrupted by the EVM for varied α. In contrast with the results shown in Fig. 3, it is observed from Fig. 5 that the maximum rate region is worse, which is dedicated by the EVM. Moreover, as the power allocation factor α increases from 0.3 to 0.4, the data rate of the NOMA-strong user is enhancing but leads to a reduction of the data rate of the NOMA-weak user. Furthermore, this result comes at the expense of different power allocation, which implies that a larger achievable rate region can be achieved when adopting appropriate power allocation schemes.

In the next comparison, the performance of the rate region in the case of half-duplex (HD)-NOMA scheme and the

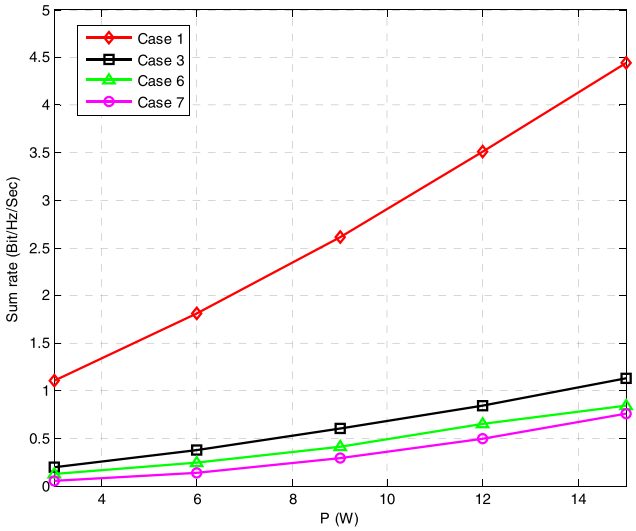

FIGURE 7. Achievable rate region of (R_1, R_2) under the four different channel conditions with weight coefficients (0.4, 0.4, 0.2) and power allocation factor α at 0.45, as well as ρ at 0.5.

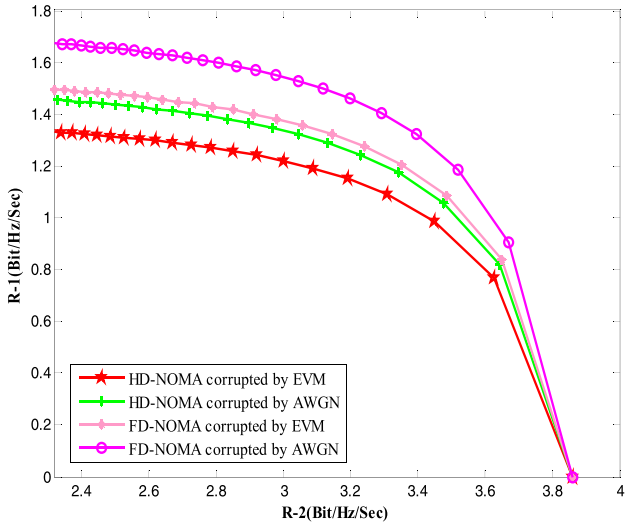

FIGURE 8. Half-duplex and full-duplex rate region comparison under the transmitted signal corrupted by the EVM and the AWGN when $R_{BS} \geq C_{12\,max}$, $R_2 \geq C_{1\,max}$.

proposed FD-NOMA is developed. One can see from Fig. 6 that the HD-NOMA method strictly performs worse than the proposed FD-NOMA scheme in terms of maximum achievable rate region. For the FD link, the rate region with $\alpha = 0.4$ is significantly larger than that of $\alpha = 0.3$. Specifically, we can further observe from Fig. 6 that the achievable rate region of the FD-NOMA scheme is still larger than the HD-NOMA one, though the power allocation coefficient of the FD-NOMA is worse than the HD-NOMA scheme, implying that the proposed FD-NOMA scheme can significantly optimize the achievable maximum rate region problem.

As indicated above, the achievable rate region of the proposed scheme is changed with different channel conditions. For the purpose of analyzing this issue, (14)-(21) are investigated, and numerical results are presented. Since numerical results are very similar, which makes it hard to distinguish different cases, we provide the sum rate optimization results of case 1, case 3, case 6 and case 7 when the transmitted power is not fixed. Additionally, the downlink rate is of great significance to the users, and the uplink rate is not depicted in our simulation results. It is observed from Fig. 7 that case 1 obviously outperforms other schemes, which is indicated by the good channel conditions of BS $\rightarrow$ U1 and U2 $\rightarrow$ BS links. In addition, when transmitted power is small, case 1 still works well. This result implies that optimizing the channel condition can improve the rate region because the inter-user interference and self-interference can be reduced.

In Fig. 8, the maximum achievable rate region of the FD-NOMA scheme and the HD-NOMA scheme with two kinds of noises are developed. Clearly, it is shown that the schemes corrupted by the EVM can lead to smaller rate regions due to the EVM deteriorating the original transmitted signal to some extent. It can also be observed from Fig. 8 that the FD-NOMA scheme corrupted by the EVM realizes a larger rate region that outperforms the two schemes with different noise based on the HD-NOMA. It should be noted that the EVM cannot be avoided in a practical FD multiple-carrier communication system, and we can conclude that the proposed FD-NOMA scheme is more reliable and efficient for achieving maximum rate region.

V. CONCLUSIONS

In this paper, the maximum achievable rate region based on NOMA has been considered. A novel cooperative FD-NOMA model with three rate region optimization schemes has been proposed. To be specific, the self–interference cancellation is deployed at the base station and the NOMA-strong user, and the data rate of the NOMA-weak user is investigated in two cases with different channel conditions. Additionally, the optimization solution is solved when the transmitted power is fixed, while two efficient algorithms are provided to optimize the achievable maximum rate region in two other cases. Furthermore, for different power allocation factors, the achievable rate region is presented with the aid of computer simulation, and it implies that we can realize different rate regions by adjusting the power allocation factor beyond the NOMA framework. Additionally, numerical results show that the EVM actually dominates the performance in terms of the rate region, and they demonstrate that the rate region of the proposed FD-NOMA scheme outperforms that of the HD-NOMA scheme. We conclude that by carefully choosing the power allocation factor and the weight coefficient, the maximum achievable rate region can be obtained beyond our expectation.

APPENDIX

For simplifying this problem, we rewrite the problem as

$$L(x) = \log_2(1 + Ax) + \log_2\left(1 + \frac{B(1-x)}{C + Bx}\right) + \lambda Dx\left(\frac{B(1-x)}{C + Bx} - Ax\right) \quad (39)$$

Here, A, B, C and D are constant. (39) can be expressed as

$$L(x) = \ln(1+Ax) + \ln\left(1+\frac{B(1-x)}{C+Bx}\right) + \lambda \ln 2Dx\left[\frac{B(1-x)}{C+Bx} - Ax\right] \quad (40)$$

Using the differential calculus theorem, we obtain

$$\frac{dL(x)}{\partial x} = \frac{1}{\ln 2}\left(\frac{A}{1+Ax} - \frac{BC+B^2}{B(C+Bx)(1-x)}\right) + \lambda D\left(\frac{B(1-x)}{C+Bx} - Ax\right) + \lambda Dx\left(\frac{-BC-B^2}{C+Bx} - A\right) \quad (41)$$

For (41), with the aids of geometric transformation, (41) can be given by

$$AB(C+Bx)(1-x) - BC(1+Ax)(B+C) + \ln 2 \times \lambda BD \times (1+Ax)(1-x)(BC - 2BCx - Cx - Bx^2) = 0 \quad (42)$$

Specifically, (41) is the condition for obtaining the extreme value. By solving (41), we obtain

$$\alpha = \frac{\sqrt{(B+AC)^2 + 4AB^2} - B - AC}{2AB} \quad (43)$$

Thus, (42) has a pole in this problem. For (42), we carry out second derivation, which is given as

$$\frac{dL^2(x)}{dx^2} = AB^2 - ABC - 2AB^2x - ABC(B+C) + \ln 2 \times \lambda BD\left((1+Ax)(1-x)(-2BC-C-2Bx) + (BC-2BCx-Cx-Bx^2)(A-2Ax-1)\right) \quad (44)$$

Using simple mathematical transformation, we finally obtain

$$\frac{dL^2(x)}{dx^2} > 0 \quad (45)$$

which is the condition of the convex problem.

REFERENCES

[1] I. Chih-Lin *et al.*, "Toward green and soft: A 5G perspective," *IEEE Commun. Mag.*, vol. 52, no. 2, pp. 66–73, Feb. 2014.

[2] G. Han, L. Liu, S. Chan, R. Yu, and Y. Yang, "HySense: A hybrid mobile crowdsensing framework for sensing opportunities compensation under dynamic coverage constraint," *IEEE Commun. Mag.*, vol. 55, no. 3, pp. 93–99, Mar. 2017.

[3] G. Han, L. Liu, J. Jiang, L. Shu, and G. Hancke, "Analysis of energy-efficient connected target coverage algorithms for industrial wireless sensor networks," *IEEE Trans. Ind. Informat.*, vol. 13, no. 1, pp. 135–143, Feb. 2017.

[4] G. Han, L. Wan, L. Shu, and N. Feng, "Two novel DOA estimation approaches for real-time assistant calibration systems in future vehicle industrial," *IEEE Syst. J.*, Jun. 2017. [Online]. Available: http://ieeexplore.ieee.org/document/7128677/, doi: 10.1109/JSYST.2015.2434822.

[5] Y. Saito, A. Benjebbour, Y. Kishiyama, and T. Nakamura, "System-level performance evaluation of downlink non-orthogonal multiple access (NOMA)," in *Proc. IEEE 24th Annu. Symp. Pers. Indoor Mobile Radio Commun.*, London, U.K., Sep. 2013, pp. 611–615.

[6] N. Zhao, X. Liu, F. R. Yu, M. Li, and V. C. M. Leung, "Communications, caching, and computing oriented small cell networks with interference alignment," *IEEE Commun. Mag.*, vol. 54, no. 9, pp. 29–35, Sep. 2016.

[7] T. Nakamura, A. Benjebbour, Y. Kishiyama, S. Suyama, and T. Imai, "5G radio access: Requirements, concept and experimental trials," *IEICE Trans. Commun.*, vol. E98, no. 8, pp. 1397–1406, 2015.

[8] T. Cover and J. Thomas, *Elements of Information Theory*, 6th ed. New York, NY, USA: Wiley, 1991.

[9] D. Tse and P. Viswanath, *Fundamentals of Wireless Communication*. Cambridge, U.K.: Cambridge Univ. Press, May 2005.

[10] Z. Ding, Z. Yang, P. Fan, and H. V. Poor, "On the performance of non-orthogonal multiple access in 5G systems with randomly deployed users," *IEEE Signal Process. Lett.*, vol. 21, no. 12, pp. 1501–1505, Dec. 2014.

[11] B. Lyu, Z. Yang, and G. Gui, "Backscatter assisted wireless powered communication networks with non-orthogonal multiple access," *IEICE Trans. Fundam. Electron., Commun. Comput. Sci.*, vol. E100-A, no. 8, pp. 1724–1728, Aug. 2017.

[12] Y. Endo, Y. Kishiyama, and K. Higuchi, "Uplink non-orthogonal access with MMSE-SIC in the presence of inter-cell interference," in *Proc. IEEE ISWCS*, Aug. 2012, pp. 261–265.

[13] X. Sun *et al.*, "Joint beamforming and power allocation design in downlink non-orthogonal multiple access systems," in *Proc. IEEE Globecom Workshops*, Washington, DC, USA, Dec. 2016, pp. 1–6.

[14] Y. Liu, Z. Ding, M. Elkashlan, and H. V. Poor, "Cooperative non-orthogonal multiple access with simultaneous wireless information and power transfer," *IEEE J. Sel. Areas Commun.*, vol. 34, no. 4, pp. 938–953, Apr. 2016.

[15] Z. Ding, M. Peng, and H. V. Poor, "Cooperative non-orthogonal multiple access in 5G systems," *IEEE Commun. Lett.*, vol. 19, no. 8, pp. 1462–1465, Aug. 2015.

[16] D. Bharadia, E. McMilin, and S. Katti, "Full duplex radios," in *Proc. ACM SIGCOMM*, Aug. 2013, pp. 375–386.

[17] D. Nguyen, L.-N. Tran, P. Pirinen, and M. Latva-Aho, "On the spectral efficiency of full-duplex small cell wireless systems," *IEEE Trans. Wireless Commun.*, vol. 13, no. 9, pp. 4896–4910, Sep. 2014.

[18] D. W. K. Ng, Y. Wu, and R. Schober, "Power efficient resource allocation for full-duplex radio distributed antenna networks," *IEEE Trans. Wireless Commun.*, vol. 15, no. 4, pp. 2896–2911, Apr. 2016.

[19] W. Li, J. Lilleberg, and K. Rikkinen, "On rate region analysis of half- and full-duplex OFDM communication links," *IEEE J. Sel. Areas Commun.*, vol. 32, no. 9, pp. 1688–1698, Sep. 2014.

[20] Z. Xiao, Y. Li, L. Bai, and J. Choi, "Achievable sum rates of half- and full-duplex bidirectional OFDM communication links," *IEEE Trans. Veh. Technol.*, vol. 66, no. 2, pp. 1351–1364, Feb. 2016.

[21] Y. Sun, D. W. K. Ng, Z. Ding, and R. Schober, "Optimal joint power and subcarrier allocation for full-duplex multicarrier non-orthogonal multiple access systems," *IEEE Trans. Commun.*, vol. 65, no. 3, pp. 1077–1091, Mar. 2017.

[22] Z. Ding, P. Fan, and H. V. Poor, "Impact of user pairing on 5G nonorthogonal multiple-access downlink transmissions," *IEEE Trans. Veh. Technol.*, vol. 65, no. 8, pp. 6010–6023, Aug. 2016.

[23] M. F. Hanif, Z. Ding, T. Ratnarajah, and G. K. Karagiannidis, "A minorization-maximization method for optimizing sum rate in the downlink of non-orthogonal multiple access systems," *IEEE Trans. Signal Process.*, vol. 64, no. 1, pp. 76–88, Jan. 2016.

[24] M. Grant and S. Boyd. (2014). *CVX: MATLAB Software for Disciplined Convex Programming, Version 2.1*. [Online]. Available: http://cvxr.com/cvx

[25] A. Georgiadis, "Gain, phase imbalance, and phase noise effects on error vector magnitude," *IEEE Trans. Veh. Technol.*, vol. 53, no. 2, pp. 443–449, Mar. 2004.

[26] J. L. Pinto and I. Darwazeh, "Error vector magnitude relation to magnitude and phase distortion in 8-PSK systems," *Electron. Lett.*, vol. 37, no. 7, pp. 437–438, Mar. 2001.

HONGJI HUANG is currently pursuing the bachelor's degree in communication engineering with the Nanjing University of Posts and Telecommunications, Nanjing, China. He has authored or co-authored several international conference papers. His research interest is 5G communications based on full duplex communications, convex optimization, and power allocation. He has participated in science research projects at College Student Innovation and Entrepreneurship Education four times (top 1%). He received the Student Award for Academy Performance (top 3%) and the First-Class Scholarship of Nanjing University of Posts and Telecommunications two times.

JIAN XIONG received the B.Sc. degree in computer science and technology from the Anhui University of Finance and Economics, Bengbu, China, in 2007, the M.Sc. degree in computer application technology from Xihua University, Chengdu, China, in 2010, and the Ph.D. degree in single and information processing from the University of Electronic Science and Technology of China, Chengdu, China, in 2015. From February 2014 to May 2014, he was a Research Assistant with the Image and Video Processing Laboratory, The Chinese University of Hong Kong, Hong Kong. Since 2015, he has been a Lecturer with the College of Telecommunications and Information Engineering, Nanjing University of Posts and Telecommunications, Nanjing, China. His current research interests include image and video coding, pattern recognition, and machine learning.

JIE YANG received the B.Sc. and M.Sc. degrees in communication engineering from the Nanjing University of Posts and Telecommunications, Nanjing, China, in 2003 and 2006, respectively, where she is currently pursuing the Ph.D. degree in communication engineering.

GUAN GUI (M'11) received the Dr.Eng. degree in information and communication engineering from the University of Electronic Science and Technology of China, Chengdu, China, in 2012. From 2009 to 2012, with financial support from the China Scholarship Council and the Global Center of Education, Tohoku University, he joined the Wireless Signal Processing and Network Laboratory (Prof. Adachi's laboratory), Department of Communications Engineering, Graduate School of Engineering, Tohoku University, as a Research Assistant and a Post-Doctoral Research Fellow, respectively. From 2012 to 2014, he was supported by the Japan Society for the Promotion of Science Fellowship as a Post-Doctoral Research Fellow with the Wireless Signal Processing and Network Laboratory. From 2014 to 2015, he was an Assistant Professor with the Department of Electronics and Information System, Akita Prefectural University. Since 2015, he has been a Professor with the Nanjing University of Posts and Telecommunications, Nanjing, China. He is currently involved in research of big data analysis, multidimensional system control, super-resolution radar imaging, adaptive filter, compressive sensing, sparse dictionary designing, channel estimation, and advanced wireless techniques.

Dr. Gui received the IEEE International Conference on Communications Best Paper Award in 2014 and 2017, and also the IEEE Vehicular Technology Conference (VTC-spring) Best Student Paper Award in 2014. He was also selected as a Jiangsu Special Appointed Professor, Jiangsu High-Level Innovation and Entrepreneurial Talent and 1311 Talent Plan in 2016. He has been an Associate Editor of the Wiley Journal *Security and Communication Networks* since 2012.

HIKMET SARI (F'95) received the Engineering degree and the Ph.D. degree from ENST, Paris, France, and the Post-Doctoral Habilitation degree from the University of Paris-Sud, Orsay. He is currently a Professor with the Nanjing University of Posts and Telecommunications, and also a Chief Scientist with Sequans Communications. He held various research and management positions in industry, including Philips Research Laboratories, SAT, Alcatel, Pacific Broadband Communications, and Juniper Networks. His distinctions include the André Blondel Medal in 1995, the Edwin H. Armstrong Achievement Award in 2003, the Harold Sobol Award in 2012, and an election to the Academy of Europe and to the Science Academy of Turkey in 2012.

He served as a Distinguished Lecturer of the IEEE Communications Society from 2001 to 2006, a member of the IEEE Fellow Evaluation Committee from 2002 to 2007, and a member of the Awards Committee from 2005 to 2007. He has served as an Editor of the IEEE TRANSACTIONS ON COMMUNICATIONS from 1987 to 1981, a Guest Editor of the *European Transactions on Telecommunications* in 1993, and the IEEE JOURNAL ON SELECTED AREAS IN COMMUNICATIONS in 1999, and an Associate Editor of the IEEE COMMUNICATIONS LETTERS from 1999 to 2002.

Prof. Sari was the Chair of the Communication Theory Symposium of ICC 2002, New York, the Technical Program Chair of ICC 2004, Paris, the Vice General Chair of ICC 2006, Istanbul, the General Chair of PIMRC 2010, Istanbul, the General Chair of WCNC 2012, Paris, the Executive Chair of WCNC 2014, Istanbul, the General Chair of ICUWB 2014, Paris, the General Co-Chair of IEEE BlackSeaCom 2015, Constanta, Romania, the Technical Program Chair of EuCNC 2015, Paris, and the Executive Co-Chair of ICC 2016, Kuala Lumpur. He also chaired the Globecom and ICC Technical Content Committee from 2010 to 2011. He was a Vice President for Conferences of the IEEE Communications Society from 2014 to 2015. He served as the General Co-Chair of ATC 2016, Hanoi, Vietnam, and the Executive Chair of ICC 2017, Paris, and is serving as the General Chair of PIMRC 2018, Istanbul.